

# p50 suppresses cytotoxic T lymphocyte effector function to regulate tumor immune escape and response to immunotherapy

Chunwan Lu,<sup>1,2,3</sup> John D Klement,<sup>1,2,3</sup> Alyssa D Smith,<sup>1,2,3</sup> Dafeng Yang,<sup>1,2,3</sup> Jennifer L Waller,<sup>4</sup> Darren D Browning,<sup>1,2</sup> David H Munn,<sup>2</sup> Kebin Liu <sup>1,2,3</sup>

**To cite:** Lu C, Klement JD, Smith AD, *et al.* p50 suppresses cytotoxic T lymphocyte effector function to regulate tumor immune escape and response to immunotherapy. *Journal for ImmunoTherapy of Cancer* 2020;**8**:e001365. doi:10.1136/jitc-2020-001365

Accepted 02 September 2020



© Author(s) (or their employer(s)) 2020. Re-use permitted under CC BY-NC. No commercial re-use. See rights and permissions. Published by BMJ.

<sup>1</sup>Department of Biochemistry and Molecular Biology, Augusta University, Augusta, Georgia, United States

<sup>2</sup>Georgia Cancer Center, Medical College of Georgia, Augusta University, Augusta, Georgia, United States

<sup>3</sup>Charlie Norwood VA Medical Center, Augusta, Georgia, United States

<sup>4</sup>Department of Population Health Sciences, Augusta University, Augusta, Georgia, United States

## Correspondence to

Dr Chunwan Lu;  
Clu@augusta.edu

Dr Kebin Liu; kliu@augusta.edu

## ABSTRACT

**Background** NF-κB is a key link between inflammation and cancer. Previous studies of NF-κB have largely focused on tumor cells, and the intrinsic function of NF-κB in T cells in tumor development and response to immunotherapy is largely unknown. We aimed at testing the hypothesis that NF-κB1 (p50) activation in T cells underlies human colon cancer immune escape and human cancer non-response to anti-PD-1 immunotherapy.

**Methods** We screened NF-κB activation in human colon carcinoma and used mouse models to determine p50 function in tumor cells and immune cells. RNA-Seq was used to identify p50 target genes. p50 binding to target gene promoters were determined by electrophoresis mobility shift assay and chromatin immunoprecipitation. A p50 activation score was generated from gene expression profiling and used to link p50 activation to T-cell activation and function pre-nivolumab and post-nivolumab immunotherapy in human patients with cancer.

**Results** p50 is the dominant form of NF-κB that is highly activated in immune cells in the human colorectal carcinoma microenvironment and neighboring non-neoplastic colon epithelial cells. Tumor cell intrinsic p50 signaling and T-cell intrinsic p50 signaling exert opposing functions in tumor growth control in vivo. Deleting *Nfkb1* in tumor cells increased whereas in T cells decreased tumor growth in preclinical mouse models. Gene expression profiling identified *Gzmb* as a p50 target in T cells. p50 binds directly to a previously uncharacterized κB sequence at the *Gzmb* promoter in T cells, resulting in repression of *Gzmb* expression in tumor-infiltrating cytotoxic T lymphocytes (CTLs) to induce a dysfunctional CTL phenotype to promote tumor immune escape. p50 activation is inversely correlated with both *GZMB* expression and T-cell tumor infiltration in human colorectal carcinoma. Furthermore, nivolumab immunotherapy decreased p50 activation and increased *GZMB* expression in human patients with melanoma.

**Conclusions** Inflammation activates p50 that binds to the *Gzmb* promoter to repress granzyme B expression in T cells, resulting in CTL dysfunction to confer tumor immune escape and decreased response to anti-PD-1 immunotherapy.

## BACKGROUND

Chronic inflammation is an established driver of human cancer.<sup>1</sup> In human patients with inflammatory disease such as ulcerative colitis, massive accumulation of immune cells, particularly T cells, immature myeloid cells and/or myeloid-derived suppressor cells is a hallmark of colonic inflammation. It has recently been determined that myeloid cells induce genome-wide DNA mutations in intestinal epithelial cells.<sup>2</sup> It is therefore not surprising that both colitis-associated human colorectal cancer and adjacent non-neoplastic colon epithelial cells from patients with colitis harbor abundant somatic mutations.<sup>3</sup> While these somatic mutations may drive epithelial cell tumorigenesis, they also serve as neoantigens to elicit tumor-reactive cytotoxic T lymphocytes (CTLs).<sup>4</sup> This is also consistent with the early findings that colon cancer is under constant host immunosurveillance by T cells.<sup>5</sup> Therefore, it might be expected that the host immune system would naturally eliminate transformed epithelial cells and early-stage tumors long before the clinically relevant tumor occurs. However, this does not happen since patients with ulcerative colitis have a significantly higher risk of developing colorectal cancer.<sup>1</sup> It is likely that colonic inflammation compromises CTL effector functions, resulting in transformed epithelial cell immune escape and tumor development despite significant tumor mutation burden that serves as neoantigens. However, this is a hypothesis that remains to be tested.

NF-κB is a key molecule that links inflammation to cancer and NF-κB deficiency in intestinal epithelial cells decreased colon tumorigenesis.<sup>6</sup> Emerging data indicate a key role of NF-κB in regulation of immune cell activation and function in the context of tumor development. It is well documented

that myeloid cell intrinsic NF- $\kappa$ B signaling promotes tumor initiation and progression.<sup>7–12</sup> NF- $\kappa$ B may directly and indirectly regulate T-cell activation, tumor infiltration and function.<sup>7–10,13–16</sup> However, polymorphisms in *NFKB1* that diminish its expression have been linked to increased risk of colorectal cancer in humans.<sup>17,18</sup> Furthermore, NF- $\kappa$ B1-deficient mice develop gastric cancer and this gastric cancer development requires loss of *Nfkb1* in both epithelial and hematopoietic cells.<sup>19</sup> This contrasting function of NF- $\kappa$ B in tumor development is at least attributed to its function in regulating T-cell tumor infiltration.<sup>12,20,21</sup> Despite these extensive studies, the intrinsic function of NF- $\kappa$ B in T cells in the context of tumor immune evasion and response to immunotherapy, however, is still incompletely understood. We report here the identification of NF- $\kappa$ B1 p50 (termed p50 thereafter) as a transcriptional repressor of *Gzmb*, the gene that encodes T-cell effector granzyme B, in T cells, and a key function of the p50–*Gzmb* axis in tumor immune evasion and response to anti-PD-1 immunotherapy.

## METHODS

### Human tumor specimens and clinical datasets

Human colon carcinoma tumor specimens and matched tumor adjacent non-neoplastic colon tissues were provided by Dr. Shannon McCall, Ms. Aubrey Coulas and Ms. Kellie Soafer at the Cooperative Human Tissue Network Southern Division (BioRepository & Precision Pathology Center, Duke University, Durham, NC). The patient pathological and treatment reports are presented in online supplemental table S1. Human colorectal cancer patient datasets were extracted from UCSC xenabrowser TCGA Colon and Rectal Cancer (COAD-READ) database. Survival analyses were calculated using the R survival and survminer packages. Datasets from human patients with melanoma with nivolumab immunotherapy were obtained from the BMS038 trial (<https://www.ncbi.nlm.nih.gov/pubmed/29033130>, GSE91061). All studies with human specimens were performed under a protocol approved by Augusta University Institutional Review Board (#1354508-1).

### Mice and cell lines

C57BL/6J, *Nfkb1* KO (p50 KO, B6.Cg-*Nfkb1*<sup>tm1Bal</sup>/J), Rel<sup>Δ</sup> mice (B6.129S1-*Rela*<sup>tm1Ukl</sup>/J) and Lck-cre (B6.Cg-Tg(Lck-cre)548Jxm/J) were obtained from the Jackson Laboratory (Bar Harbor, ME). WT and p50 KO chimera mice were created by adoptively transferring bone marrow cells from WT and p50 KO mice to lethally irradiated (900 RAD) recipient C57BL/6J mice. All animal studies are approved in advance by Augusta University Institutional Animal Care and Use Committee. The murine colon epithelial cell line MC38 were provided by Dr. Jeffrey Schlom. EL4 T cells were obtained from ATCC.

### Mouse tumor models

Mice were injected with azoxymethane (AOM, Sigma-Aldrich, 10 mg/kg body weight) intraperitoneally once, followed by administration of 2% dextran sulfate sodium (DSS; MP Biomedicals, Santa Ana, CA) through the drinking water 1 day later for 1 week. DSS was replaced with water for 2 weeks. The DSS/water cycle was repeated two more times. Mice were maintained with regular drinking water for one more month after the third cycle and then sacrificed for analysis. Colon tissues were dissected from the mice, flushed and cleaned with PBS, and cut open longitudinally to examine tumor nodules. Anti-PD-1 immunotherapy in the MC38 tumor model was performed as previously described.<sup>22</sup>

### RNA sequencing and p50 signature gene panel identification

RNA was purified from tumor tissues collected from the AOM–DSS-induced tumors in WT and p50 KO mice. RNA-Seq was performed in Novogene Corp. Genes in p50 score were identified as those having >2-fold change in expression and adjusted p value <0.05. Genes were then filtered to known human NF- $\kappa$ B targets using an online database (<https://www.bu.edu/nf-kb/gene-resources/target-genes/>). p50 score was calculated using the sing-score R package.

### Flow cytometry, RT-PCR analysis and Western blotting analysis

Flow cytometry, NF- $\kappa$ B activation, RT-PCR and Western blotting analysis were performed as previously described.<sup>23</sup> The sequences of primers are listed in online supplemental table S2. All antibodies are listed in online supplemental table S3.

### Electrophoresis mobility shift assay (EMSA)

Eight putative  $\kappa$ B DNA sequences at the *Gzmb* promoter region were identified using the MacVector program (Apex, NC). These sequences are for all NF- $\kappa$ B subunits. Oligonucleotides were synthesized based on these sequences. The DNA probes containing these  $\kappa$ B sequences are P1 (GAGGGCAGAGGTCTTTCTCAG), P2 (TTGGGAAAGTGTCAATTGTAG), P3 (GCAAAGTGATCTTCCTAGAA), P4 (CATAGAATCCTCTAGATGCTA), P5 (CAGTCAGTGATTCCACTTTCA), P6 (TCTGCAAAGTGGATCTTCTCA), P7 (GTGTTGGA GCTTTCCATTTAT) and P8 (CAGAAGGAAATTTCCC AAATC). The positive control  $\kappa$ B probe sequence is AGTTGAGGGGACTTTCCCAGGC (Santa Cruz cat no. sc-2505). The end-labeled probes were incubated with nuclear extracts with IgG or specific antibodies and analyzed.

### Chromatin immunoprecipitation (ChIP)

ChIP was performed using anti-p50 (Santa Cruz) and the Chromatin Immunoprecipitation (ChIP) Assay Kit (Millipore, Burlington, MA) according to the manufacturer's instructions. Normal rabbit IgG (Santa Cruz Biotechnology, Dallas, TX) was used as negative control for the antibody. The immunoprecipitated genomic DNA was amplified by qPCR using PCR primers (online

supplemental table S2) covering the region of the *Fas* and *Gzmb* promoter regions.

### Immunohistochemistry

Immunohistochemistry was performed essentially as described previously.<sup>22</sup> Human and mouse tissue sections were probed with Anti-p50 antibody (Santa Cruz) overnight at 4°C, followed by incubation with HRP Universal Anti-Mouse/Anti-Rabbit IgG Antibody (Vector Laboratories, Burlingame, CA) according to the manufacturer's instructions.

### Statistical analysis

Statistical comparisons between any two groups were conducted using unpaired two-tailed Student t-test and p values were indicated in their corresponding graphs. GraphPad Prism program was used to analyze correlation and linear regression. P values <0.05 were considered as statistically significant, and error bars are indicated as mean±SD. Two-factor analysis of variance using SAS V.9.4 and an overall alpha level of 0.05 was performed to examine the effect of treatment on tumor volume and weight between the WT and p50 KO mice. The main effects of mouse strain and treatment and two-factor interaction were included in each model, and the statistical test of interest was the F-test for the two-factor interaction. A Tukey multiple comparison procedure was used to examine post hoc differences between mouse strain and treatment groups.

## RESULTS

### Colonic inflammation preferentially activates p50 in colonic and tumor microenvironment

The subunits of NF-κB complexes have contrasting functions in tumor development.<sup>12 14 15 19 24</sup> We first aimed at profiling inflammation-driven NF-κB activation using a DNA probe with κB consensus sequence for all five Rel subunits. In the colitis model, p50 activation was predominant in the inflamed non-neoplastic colon over the other four NF-κB Rel subunits (figure 1A). A similar p50 activation profile was also observed in the colon carcinoma of the AOM–DSS colon cancer model (figure 1B). It seems that p50 also primarily exist as p50–p50 homodimer in the inflamed colon and colon carcinoma since no significant activation of the other four Rel subunits were detected (figure 1A,B). DSS-mediated inflammation induced p50 activation in the colon in a time-dependent manner (figure 1C, online supplemental figure S1). In addition, the degree of colonic inflammation is correlated with p50 activation (online supplemental figure S1). The p50 protein level also increased with time and correlated with increased activation and the degree of colonic inflammation (online supplemental figure S1). The colon-infiltrating immune cells have higher level of p50 protein than the colon epithelial cells (online supplemental figure S1).

Ten matched pairs of human colon carcinoma and adjacent non-neoplastic colon tissues were analyzed by immunohistochemistry. The nuclear staining of p50 was analyzed and used as marker of p50 activation in epithelial, tumor and immune cells. p50 protein level is higher in colon epithelial cells than in tumor cells (figure 1D,E) and also p50 activation level is higher in colon epithelial cells than in the tumor cells (figure 1D,E). Furthermore, immune cells have higher p50 activation than epithelial cells and tumor cells, respectively (figure 1D,E). As a complimentary approach, analysis of p50 mRNA expression level of human colorectal carcinoma and adjacent non-neoplastic colon from the TCGA database also determined that p50 expression level is significantly higher in the adjacent non-neoplastic colon tissue than in colorectal carcinoma in human patients with colorectal cancer (figure 1F).

### p50 promotes tumorigenesis and growth through an immune cell-dependent mechanism

The p50 NF-κB has a contrasting role in tumor development.<sup>12 14 15 17–19 24–27</sup> We next aimed at determining the function of p50 in colon tumorigenesis. Colon tumorigenesis incidence was significantly lower in mice with global p50 deficiency as compared with WT mice (figure 2A). p50 deficiency also resulted in a significant decrease in Methylcholanthrene (MCA)-induced tumorigenesis (figure 2B). However, chimera mice with p50 deficiency only in immune cells also exhibited a significant decrease in colon tumorigenesis incidence (figure 2C). Consistent with p50 intrinsic function in immune cells as a tumor promoter, p50-sufficient colon tumor grew significantly slower in mice with p50 deficiency as compared with WT mice (figure 2D,E). We next took advantage of the existing p65-floxed mice and generated mice with p65 deficiency only in T cells (p65 TKO mice). As observed in the p50 chimera mice, the p65 TKO mice developed significantly less tumor than the control mice (figure 2F).

### p50 tumor intrinsic signaling suppresses colon tumor growth in vivo

To dissect the relative functions of p50 in tumor cells from immune cells, *Nfkb1* gene was knocked out in CT26 cells using CRISPR (online supplemental figure S2A). EMSA confirmed that p50 activation is diminished in p50 KO CT26 cells (online supplemental figure S2A). Interestingly, the p65 NF-κB activation was also diminished in the p50 KO tumor cells (online supplemental figure S2A). In contrast to what was observed in p50 global KO mice, knocking out p50 only in tumor cells significantly increased tumor nodule number in WT mice (online supplemental figure S2B). As in the CT26 cells, p65 activation was also diminished in the p50-deficient MCA tumor cells (online supplemental figure S2C). Again, p50 deficiency only in tumor cells significantly increased tumor growth in vivo (online supplemental figure S2D & 2E). We next blocked the canonical NF-κB activation in CT26 and MC38-met tumor cells using the IκBα-AA



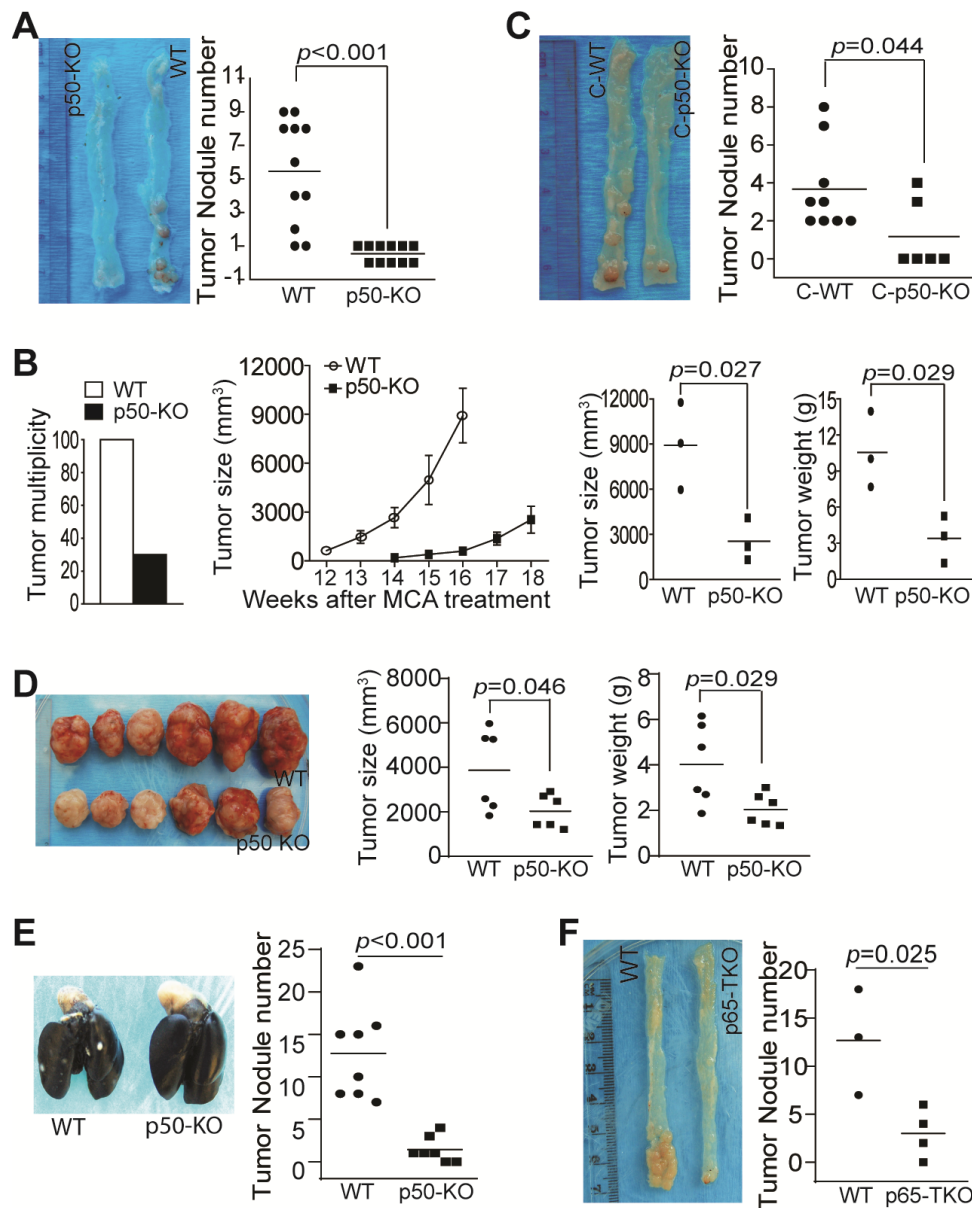


**Figure 2** NF- $\kappa$ B negatively regulates T-cell function to promote colon tumorigenesis and growth in vivo. (A) WT (n=11) and p50 KO (n=11) mice were treated with the AOM–DSS cycles. Shown are representative images of tumor-bearing colon tissues and quantification of tumor nodules of pooled results of two independent experiments. (B) WT (n=10) and p50 KO (n=10) mice were treated with MCA. The tumor incidence was determined at the end of the experiments (left panel). Seven WT mice were sacrificed before 12 weeks due to large tumor size. Only the last three WT mice were monitored for tumor growth. Only three of the 10 p50 KO mice developed tumor. Tumor growth was monitored starting at week 14. These three mice were sacrificed at week 18 (middle panel). The tumor size and weight from the three WT and three p50 KO mice were determined at week 16 (WT mice) and week 18 (p50 KO mice) and quantified (right two panels). (C) The WT (n=9) and p50 KO (n=6) chimera mice were treated with the AOM–DSS cycles. Shown are representative images of tumor-bearing colon tissues. The tumor nodule numbers were quantified and presented in the right panel. (D) WT (n=6) and p50 KO (n=6) mice were injected with MC38 cells subcutaneously. Shown are representative images of MC38 tumors (left panel). The tumor size and tumor weight were measured and presented in the right panel. (E) WT (n=8) and p50 KO (n=7) mice were injected with MC38-met cells intravenously. Lungs were collected 16 days later and inflated with ink. Shown are representative images of tumor-bearing lungs and quantification of tumor nodule number. (F) WT (*Lck-cre*, n=3) and p65 TKO (n=4) mice were treated as in (A). Shown are representative images of tumor-bearing colon tissues from WT and p65 TKO mice (left panel) and quantification of tumor nodules (right panel).

further analyzed these genes in tumor-infiltrating CD45<sup>+</sup> cells. Five genes were upregulated and four genes were downregulated in p50 KO tumor-infiltrating CD45<sup>+</sup> cells as compared with WT CD45<sup>+</sup> cells (figure 3E). One of the

upregulated genes is *Gzmb* (figure 3C–E). p50 negatively regulates granzyme B<sup>+</sup> tumor-infiltrating CTLs.

Granzyme B is the master CTL effector that executes CTL anti-tumor cytotoxicity.<sup>29</sup> The aforementioned

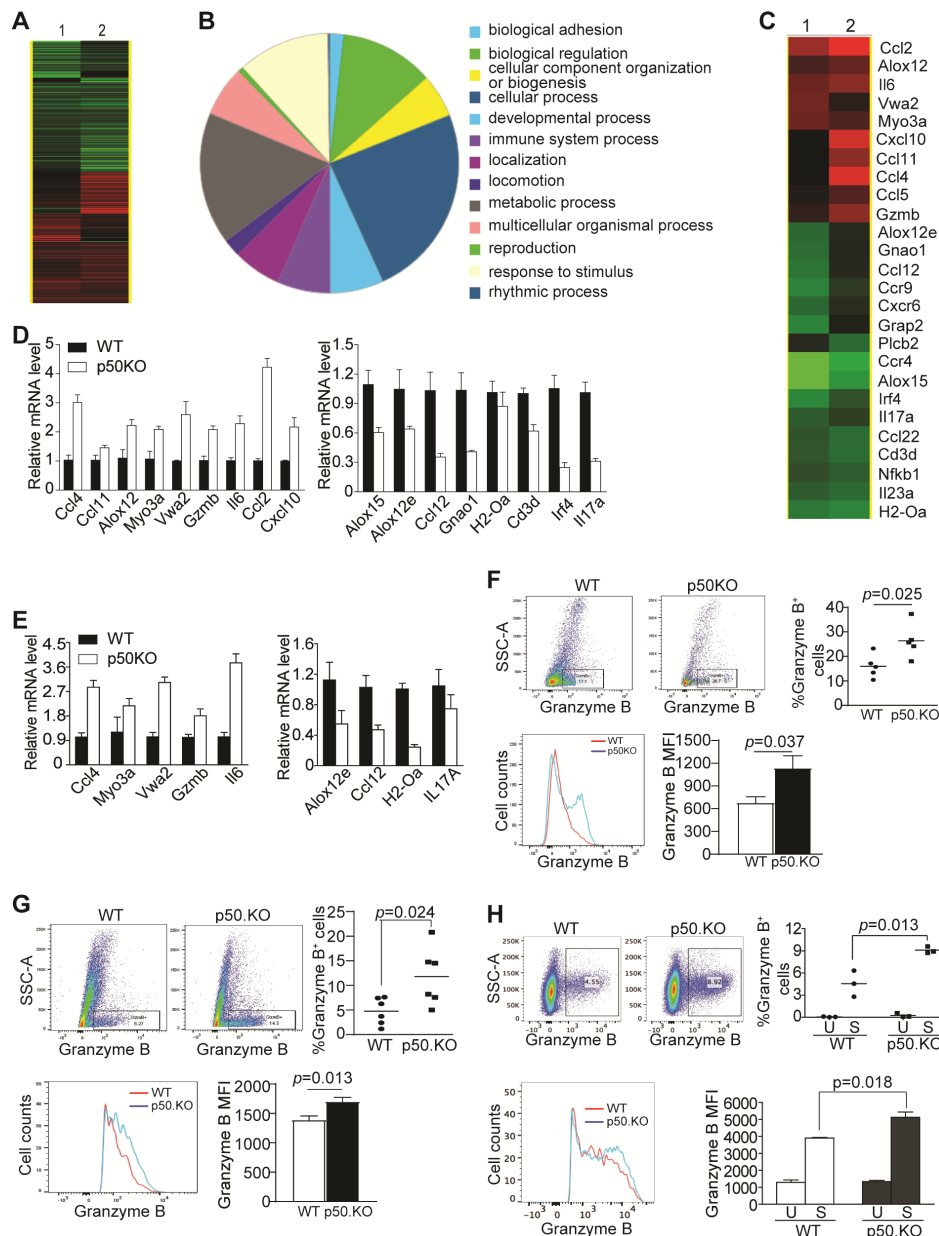


**Figure 3** p50 represses *Gzmb* expression in CD8<sup>+</sup> T cells. (A) RNA-Seq analysis of AOM-DSS-induced tumors of WT (n=2) and p50 KO (n=2) mice as shown in figure 2A. (B) The differentially expressed genes were functionally grouped. (C) Genes with known functions in the immune system were then clustered and presented. (D) The expression levels of the genes as shown in (C) were analyzed by qPCR. Shown are validated genes. (E) CD45<sup>+</sup> cells were isolated from the colon tumor tissues as in figure 2D. RNA was isolated from the purified tumor-infiltrating CD45<sup>+</sup> cells and analyzed by qPCR for the expression levels of genes shown in (D). The validated genes are shown. (F) MC38 tumors as shown in figure 2D were collected from WT (n=6) and p50 KO (n=6) mice and analyzed by flow cytometry. The live cells were gated for CD45.2<sup>+</sup> and CD8<sup>+</sup> cells. The CD8<sup>+</sup> cells were then gated for granzyme B<sup>+</sup> cells and granzyme B MFI in CD8<sup>+</sup>granzyme B<sup>+</sup> cells. Shown are representative dot plots of granzyme B staining (upper left panels) and quantification of % granzyme B<sup>+</sup> cells (upper right panel). Each dot represents one mouse. The CD8<sup>+</sup>granzyme B<sup>+</sup> cells were also quantified for granzyme B MFI and shown as overlay (bottom left panel) and quantification (bottom right panel). (G) MC38 tumor cells were surgically transplanted to cecal wall of WT (n=5) and p50 KO (n=5) mice. The orthotopic tumors were collected 30 days later and analyzed for granzyme B<sup>+</sup> cells in CD8<sup>+</sup> tumor-infiltrating T cells as in (F). (H) CD3<sup>+</sup> T cells were purified from spleens of WT (n=3) and p50 KO (n=3) mice and stimulated in anti-CD3 and anti-CD28-coated plates for 3 days. The unstimulated cells (U) and the stimulated cells (S) were stained with anti-CD8 and anti-granzyme B mAbs and analyzed by flow cytometry.

observations prompted us to test the hypothesis that p50 negatively regulates *Gzmb* expression to decrease granzyme B<sup>+</sup> tumor-infiltrating CTLs to promote tumor development. To test this hypothesis, tumor-infiltrating

CD8<sup>+</sup> T cells were analyzed for granzyme B expression. It is clear that granzyme B<sup>+</sup> tumor-infiltrating CD8<sup>+</sup> T-cell level is significantly higher in p50-deficient mice than in WT mice (figure 3F,G). Granzyme B protein level of these

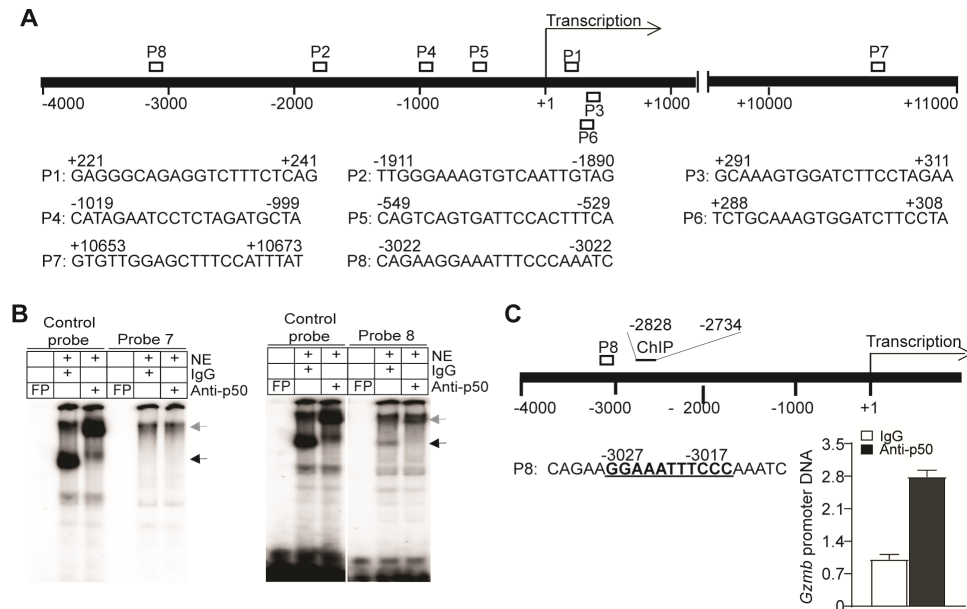


**Figure 4** p50 binds to a  $\kappa$ B sequence element in the *Gzmb* promoter to repress *Gzmb* expression in T cells. (A) The structure of the mouse *Gzmb* promoter region showing the putative NF- $\kappa$ B-binding sequences (P1–8) and locations. (B) Nuclear extracts were prepared from EL4 T cells and analyzed by EMSA using putative *Gzmb* promoter DNA probes 7 and 8 as shown in (A). The NF- $\kappa$ B consensus sequence probe (control probe) was used as positive control. The black arrow indicates the NF- $\kappa$ B–DNA complex and the gray arrow indicates p50 mAb-induced supershift. Shown are p50 binding to probe 8. Probe 7 is shown here as a negative control. (C) The left panel shows the mouse *Gzmb* promoter structure. The putative NF- $\kappa$ B-binding sequence (P8) and the ChIP PCR primer sequence locations are shown. The numbers under the bar and above the P8 probe sequence indicate the nucleotide locations relative to *Gzmb* transcription start site. EL4 T cells were analyzed by ChIP using IgG and p50-specific antibody, respectively. The immunoprecipitated DNA were quantified by qPCR using primers that amplify the *Gzmb* promoter DNA as shown at the left panel.

CD8<sup>+</sup> granzyme B<sup>+</sup> CTLs is also significantly higher in p50-deficient mice than in WT mice (figure 3F,G). In vitro activated p50-deficient CD8<sup>+</sup> T cells also have a significantly higher level of granzyme B<sup>+</sup> cells than those of WT CD8<sup>+</sup> T cells (figure 3H). The granzyme B Mean Fluorescence Intensity (MFI) is also higher in p50-deficient CD8<sup>+</sup> T cells than that in the WT CD8<sup>+</sup> T cells (figure 3H). Taken together, our findings indicate that p50 represses *Gzmb* expression in tumor-infiltrating CTLs.

#### p50 binds to a $\kappa$ B element at the *Gzmb* promoter to repress *Gzmb* expression in T cells

The previously mentioned observations indicate that p50 may directly repress *Gzmb* expression in T cells. We screened the murine *Gzmb* promoter DNA sequence and identified eight putative  $\kappa$ B consensus sequence elements (figure 4A). Analysis of DNA–protein interaction using these  $\kappa$ B sequence-containing DNA probes and T-cell nuclear extracts determined that p50 binds to one of these eight putative  $\kappa$ B DNA elements (figure 4B and online supplemental figure S5). ChIP analysis determined that p50 binds to the chromatin region containing this unique  $\kappa$ B DNA sequence at the *Gzmb* promoter in T cells (figure 4C). Taken together, we have identified a previously uncharacterized  $\kappa$ B sequence element in the *Gzmb* promoter and determined that p50 directly binds to this specific  $\kappa$ B DNA sequence at the *Gzmb* promoter to repress *Gzmb* expression in T cells.

#### *GZMB* expression and T-cell infiltration is negatively regulated by p50 in human colorectal carcinoma

To determine whether the aforementioned findings can be translated to human cancer, we analyzed the genomic dataset in human TCGA database. Because *Gzmb* is repressed by p50 in mouse colon carcinoma, we focused on p50-repressed genes. We extracted the top upregulated genes in p50 KO tumor from our RNA-Seq dataset (figure 3A) and filtered out these genes against the known human NF- $\kappa$ B target genes.<sup>30</sup> Twenty-one human genes were generated and defined as p50 signature (figure 5A,B). We defined p50 score as the level of upregulation of these 21 p50 signature genes in p50 KO tumor. The lower the p50 signature gene expression, the higher p50 activation/p50 score. As observed in mouse models, p50 activation is higher in tumor adjacent non-neoplastic colon tissues as compared with the tumor tissues in human patients with colorectal cancer since p50 score is lower in colorectal carcinoma than in adjacent non-neoplastic colon tissues (figure 5C). Furthermore, p50 score is inversely correlated with *GZMB* expression level in human colorectal carcinoma (figure 5D), indicating that p50 represses *GZMB* expression in human colorectal carcinoma.

To determine whether p50 regulates T-cell tumor infiltration in human patients with colorectal cancer, we used the CIBERSORT algorithm to deconvolute CD8<sup>+</sup>

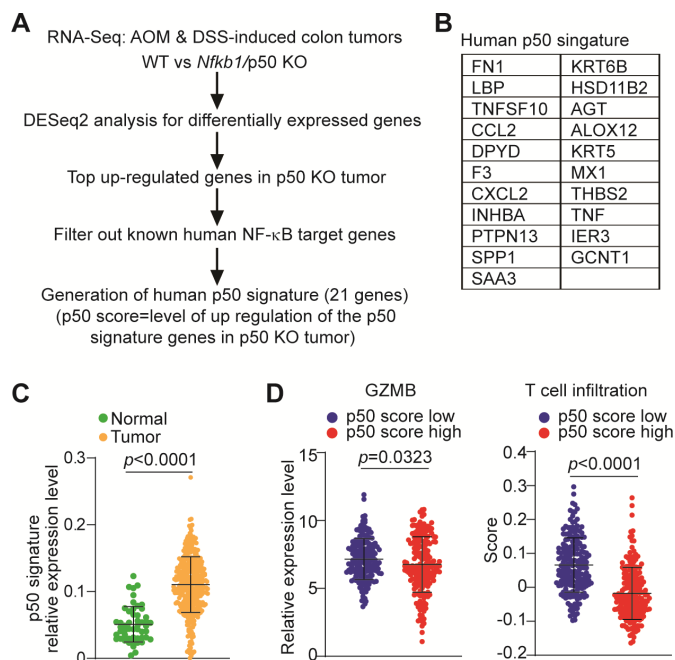


**Figure 5** p50 activation and function in human colorectal carcinoma. (A) Experimental scheme of determination of the p50 signature in human colorectal carcinoma. (B) The 21 human genes for p50 signature. The p50 score is defined as the upregulation level of the 21 human p50 signature genes in p50 KO tumor. (C) Datasets of the p50 signature genes as listed in (B) in human colon carcinoma (n=380) and normal colon tissues (n=51) were extracted from TCGA database and plotted. The p50 signature gene mRNA level was compared between colon carcinoma and normal colon tissues. Two-tailed t-tests were used to determine differences with  $p < 0.05$  as being statistically significant. (D) Datasets of human colorectal carcinoma (n=380) were extracted from TCGA database and divided into p50 score high (p50 signature expression low, n=190) and p50 score low (p50 signature high, n=190) group, and analyzed for *GZMB* mRNA level and the CD8<sup>+</sup> T-cell infiltration level. Two-tailed t-tests were used to determine differences with  $p < 0.05$  as being statistically significant.

T-cell infiltration.<sup>31</sup> p50 score high human colorectal carcinomas have a lower T-cell infiltration and p50 score low human colorectal carcinoma exhibit a higher T-cell infiltration (figure 5D). This finding indicates that p50 suppress T-cell tumor infiltration in human colorectal carcinoma.

### Anti-PD-1 immunotherapy efficacy and p50-mediated immune suppression

Our previously mentioned observations suggest that p50 activation may negatively regulate cancer patient response to anti-PD-1 immunotherapy. To test this hypothesis, we used WT and p50 KO mice to test the efficacy of anti-PD-1 immunotherapy in the MC38 tumor model. MC38 is a type of tumor that is responsive to anti-PD-1 immunotherapy.<sup>32</sup> As expected, anti-PD-1 immunotherapy significantly suppressed the MC38 colon tumor growth in WT mice (figure 6A,B). p50 KO mice also showed a significantly decreased tumor growth as compared with the WT

mice (figure 6A,B). However, anti-PD-1 immunotherapy did not further suppress the established MC38 tumor growth (figure 6A,B).

A statistically significant two-factor interaction between mouse strains and treatment was found for tumor volume ( $F(1,16)=11.45$ ,  $p=0.0038$ ) (online supplemental table S4). Tumor volumes were higher with IgG treatment than with anti-PD-1 immunotherapy in WT mice, but in p50 KO mice tumor volumes were slightly lower with IgG treatment than with anti-PD-1 immunotherapy. The Tukey multiple comparison post hoc tests indicated that IgG control mice had significantly higher tumor volumes than mice with anti-PD-1 immunotherapy ( $p=0.0034$ ) and IgG control p50 KO mice ( $p=0.0192$ ). There were no other significant differences (WT mice with anti-PD-1 vs p50 KO mice with anti-PD-1 ( $p=0.4958$ ), WT mice with anti-PD-1 vs IgG control p50 KO mice with anti-PD-1 ( $p=0.0604$ ), p50 KO mice with anti-PD-1 vs p50 KO mice with IgG ( $p=0.9345$ )) (figure 6B).

A statistically significant two-factor interaction between strain and treatment was found for tumor weight ( $F(1,16)=18.21$ ,  $p=0.0006$ ) (online supplemental table S4). Tumor weight was higher in IgG control WT mice than with anti-PD-1-treated WT mice, but in p50 KO mice tumor weight was slightly lower with IgG than with anti-PD-1 treatment. The Tukey multiple comparison post hoc tests indicated that IgG control WT mice had significantly higher tumor weight than WT mice with anti-PD-1 immunotherapy ( $p=0.0003$ ), p50 KO mice with anti-PD-1 immunotherapy ( $p=0.0225$ ) and IgG control p50 KO mice ( $p=0.0075$ ). There were no other significant differences (WT mice with anti-PD-1 vs p50 KO mice with anti-PD-1 ( $p=0.1586$ ), WT mice with anti-PD-1 vs IgG control p50 mice ( $p=0.3637$ ), p50 KO mice with anti-PD-1 vs IgG control p50 KO mice ( $p=0.9475$ )) (figure 6B).

There is a rich literature of immune checkpoint immunotherapy datasets from human patients with melanoma.<sup>33,34</sup> To determine the role of p50 in human patients who respond to anti-PD-1 immunotherapy, we analyzed p50 activation and *GZMB* expression in human melanoma patient specimens taken pre-immunotherapy and during immunotherapy. Nivolumab immunotherapy significantly decreased p50 activation and increased *GZMB* expression in human patients with melanoma (figure 6C). Furthermore, *GZMB* expression level is inversely correlated with p50 activation level (figure 6D), and nivolumab-induced increase in *GZMB* expression level is significantly correlated with decreased p50 activation in human patients with melanoma (figure 6E).

In summary, our data indicate that inflammation in the tumor microenvironment activates p50 NF-κB that represses *GZMB* expression in tumor-infiltrating CTLs to induce CTL exhaustion/dysfunction. Anti-PD-1 immunotherapy may act through unleashing the p50-suppressed dysfunctional CTL subsets of tumor-infiltrating CTLs to suppress tumor growth.

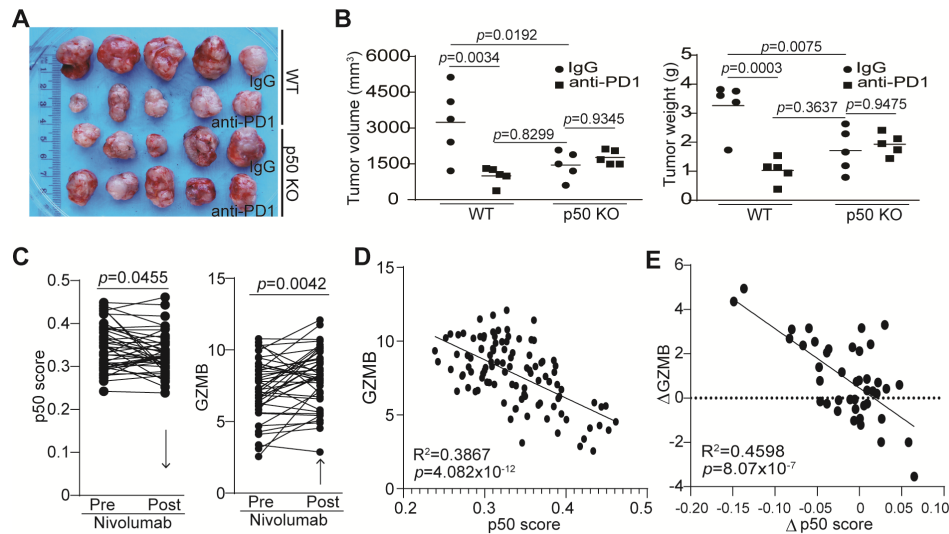


**Figure 6** p50 represses *GZMB* expression to regulate tumor response to anti-PD-1 immunotherapy. (A) MC38 tumor-bearing WT (n=10) and p50 KO (n=10) mice were randomly assigned into two groups (n=5 per group) at day 8 after tumor cell injection. One group of WT and p50 KO mice were treated with IgG, and the other group of WT and p50 KO mice were treated with anti-PD-1 (200  $\mu$ g/mouse) every 3 days for 14 days. Shown are tumor images. (B) Mice were sacrificed at day 22 after tumor cell injection. Tumors were dissected and measured for volume (left panel) and weight (right panel). (C) Datasets of the p50 signature genes (p50 score) and *GZMB* in tumors from human patients with melanoma before and after anti-PD-1 immunotherapy (n=42) were obtained from the BMS038 trial. The expression levels of p50 signature genes (p50 score, left panel) and *GZMB* (right panel) for each patient were compared. Arrows indicate net change pre-nivolumab and post-nivolumab therapy. (D) p50 signature gene level and *GZMB* of human melanoma (n=107) were plotted. The correlation between p50 score and *GZMB* expression was analyzed (left panel). (E) The change in *GZMB* expression level post anti-PD1 immunotherapy (*GZMB* expression level post-therapy–*GZMB* expression level pre-therapy) and the change of p50 score post anti-PD-1 immunotherapy (p50 score post-therapy–p50 score pre-therapy) were analyzed for correlation by linear regression using GraphPad Prism program (n=42).

## DISCUSSION

A recent study determined that both human colitis-associated colorectal tumor cells and adjacent non-tumor epithelial cells harbor a high tumor mutation burden.<sup>3</sup> Although these mutations may drive tumor development, recent studies have also shown that higher nonsynonymous mutations in tumor cells may serve as neoantigens to elicit anti-tumor immune response.<sup>35</sup> These findings indicate that the host cancer immunosurveillance may be activated long before the mutated/transformed colon epithelial cells develop into tumor cells in the inflamed colon. However, the immunogenic colorectal cancer is not naturally eliminated. Both Microsatellite Instability (MSI) and Microsatellite Stability (MSS) human colon cancer harbor abundant CTLs.<sup>22</sup> However, the majority of human colon cancers (eg, MSS colon cancer) do not respond to anti-PD-1 immunotherapy, suggesting that the tumor-infiltrating CTLs are functionally impaired. Our findings that p50 expression and activation level is significantly higher in tumor-infiltrating and adjacent non-neoplastic colonic immune cells in human patients with colorectal cancer suggest that colonic inflammation may preferentially activate p50 to induce CTL dysfunction, leading to impaired CTL function and resultant immune escape of transformed colon epithelial cells and tumorigenesis. This notion is also supported by our findings that *GZMB* expression is downregulated and T-cell infiltration

is decreased in human colorectal carcinoma with higher p50 activation level than those with lower p50 activation level.

Although the function of and mechanism underlying NF- $\kappa$ B in tumor development have been largely focused on tumor cells, recent studies have started to shed light on the critical role of NF- $\kappa$ B in regulation of anti-tumor immunity.<sup>7–16 36</sup> Specifically, a recent CRISPR-based systemic immunotherapy target screening identified NF- $\kappa$ B as the strongest potential regulator of CTL effector function.<sup>13</sup> In this study, we extended p50 function to T-cell anti-tumor effector function and determined that p50 directly represses *Gzmb* expression in T cells to decrease *Gzmb*<sup>+</sup> CTLs in the tumor microenvironment. Furthermore, we identified a previously uncharacterized  $\kappa$ B element in the *Gzmb* promoter and functionally determined that p50 directly binds to this  $\kappa$ B element in the *Gzmb* promoter to repress *Gzmb* transcription in T cells.

T-cell exhaustion/dysfunction is characterized by PD-1 upregulation that is a consequence of chronic inflammation during viral infection and is associated with the tumor microenvironment.<sup>23 37–42</sup> *Gzmb*<sup>lo</sup> has recently been proposed as a dysfunctional CTL phenotype.<sup>41</sup> Our findings thus suggest that the p50 may confer tumor-infiltrating CTL a *Gzmb*<sup>lo</sup> exhaustion/dysfunctional phenotype and immune checkpoint inhibitor



immunotherapy activates this *Gzmb*<sup>lo</sup> subset of T cells to suppress tumor.

Only subsets of CTLs respond to immune checkpoint inhibitor immunotherapy.<sup>41–43</sup> In this study, we observed that anti-PD-1 immunotherapy in tumor-bearing WT and p50 deficiency mice have similar efficacy in suppressing colon tumor growth in vivo. However, p50 deficiency and anti-PD-1 immunotherapy did not show additive or synergistic efficacy. This observation suggests that p50 deficiency and anti-PD-1 immunotherapy may activate the same subset of CTLs in the colon tumor microenvironment. This notion is supported by the clinical findings that nivolumab immunotherapy decreased p50 activation and increased *Gzmb* expression in human melanoma, a responder type of human cancer to immune checkpoint inhibitor immunotherapy.<sup>34–40–44</sup>

NF- $\kappa$ B functions as dimers. The five NF- $\kappa$ B Rel family subunits can form dimers in any combinations and 10 dimers have been identified so far including p50–p50 dimers.<sup>45</sup> In this study, we determined by EMSA that the NF- $\kappa$ B in the inflamed colon and colon carcinoma is primarily p50–p50 dimer. Furthermore, this p50–p50 dimer acts as a repressor for *Gzmb* transcription in T cells. The mechanism underlying the preferential activation of p50 in the colon and T cells requires further studies. NF- $\kappa$ B activation is a key link between colonic inflammation and colorectal cancer in humans.<sup>1</sup> NF- $\kappa$ B is activated by colonic inflammatory mediators. Emerging experimental data indicate that innate lymphoid cells (ILCs) play a critical role in colonic inflammation and colon tumorigenesis.<sup>46–47</sup> Furthermore, intestinal ILCs produce IL17<sup>48</sup> and IL17 has been shown to activate NF- $\kappa$ B in immune cells.<sup>49</sup> It is therefore possible that colitis-associated ILCs may contribute to p50 NF- $\kappa$ B activation in the inflamed colon. However, the role of the ILC-IL17 axis in inducing p50 NF- $\kappa$ B activation in CTLs in the inflamed colon and colon tumor remains to be determined. Furthermore, a recent study has shown that ILCs express PD-L1 and conditional deletion of ILC-expressed PD-L1 impairs T-cell differentiation and cytokine production.<sup>50</sup> It is therefore also possible that anti-PD-1 immunotherapy may target ILC-expressed PD-L1 to suppress production of cytokines such as IL17 to inhibit NF- $\kappa$ B activation, resulting in increased *Gzmb* expression in CTLs, which also remains to be determined. Nonetheless, our findings suggest that selective targeting of p50 activation in CTLs in the inflamed tumor microenvironment is potentially an effective strategy to reverse CTL dysfunction to restore host cancer immune surveillance to suppress tumorigenesis and progression.

## CONCLUSION

p50 binds to the *Gzmb* promoter to repress *Gzmb* transcription in T cells to induce CTL dysfunction to promote tumor immune escape. p50 activation is inversely correlated with both *GZMB* expression and T-cell tumor infiltration levels in human colorectal carcinoma. Furthermore, *GZMB* expression level is also inversely correlated

with p50 activation in human melanoma and nivolumab immunotherapy significantly decreased p50 activation to increase *GZMB* expression in responder patients with melanoma. Our data indicate that selectively targeting the p50–*GZMB* axis is potentially an effective approach to suppress cancer immune escape and to enhance the efficacy of anti-PD-1 immunotherapy.

**Acknowledgements** We thank Ms. Penny Roon and Donna Kumiski at the Medical College of Georgia Electron Microscopy and Histology Core for technical assistance in tissue preparation and histology work.

**Contributors** CL, DDB, DHM, KL: concept and design. CL, JDK: development of methodology. CL, JDK, ADS, DY: acquisition of data. CL, JDK, JLW, DDB, DHM, KL: analysis and interpretation of data. CL, JDK, DDB, DHM, KL: writing and review of manuscript.

**Funding** This work was supported by the National Institutes of Health (R01 CA182518, R01 CA133085 and R01 CA227433 to KL; F30 CA236436 to JDK) and US Department of Veterans Affairs (CX001364 to KL).

**Competing interests** None declared.

**Patient consent for publication** Not required.

**Ethics approval** Augusta University IACUC Protocol No. 2008-0162.

**Provenance and peer review** Not commissioned; externally peer reviewed.

**Data availability statement** All data relevant to the study are included in the article or uploaded as online supplemental information.

**Open access** This is an open access article distributed in accordance with the Creative Commons Attribution Non Commercial (CC BY-NC 4.0) license, which permits others to distribute, remix, adapt, build upon this work non-commercially, and license their derivative works on different terms, provided the original work is properly cited, appropriate credit is given, any changes made indicated, and the use is non-commercial. See <http://creativecommons.org/licenses/by-nc/4.0/>.

## ORCID iD

Kebin Liu <http://orcid.org/0000-0003-1965-7240>

## REFERENCES

- Lasry A, Zinger A, Ben-Neriah Y. Inflammatory networks underlying colorectal cancer. *Nat Immunol* 2016;17:230–40.
- Canli Özge, Nicolas AM, Gupta J, et al. Myeloid cell-derived reactive oxygen species induce epithelial mutagenesis. *Cancer Cell* 2017;32:869–83. e865.
- Baker A-M, Cross W, Curtius K, et al. Evolutionary history of human colitis-associated colorectal cancer. *Gut* 2019;68:985–95.
- Capietto A-H, Jhunjhunwala S, Pollock SB, et al. Mutation position is an important determinant for predicting cancer neoantigens. *J Exp Med* 2020;217:e20190179.
- Van den Eynde M, Mlecnik B, Bindea G, et al. The link between the Multiverse of immune microenvironments in metastases and the survival of colorectal cancer patients. *Cancer Cell* 2018;34:1012–26.
- Greten FR, Eckmann L, Greten TF, et al. Ikkbeta links inflammation and tumorigenesis in a mouse model of colitis-associated cancer. *Cell* 2004;118:285–96.
- Suresh R, Barakat DJ, Barberi T, et al. NF- $\kappa$ B p50-deficient immature myeloid cell (p50-IMC) adoptive transfer slows the growth of murine prostate and pancreatic ductal carcinoma. *J Immunother Cancer* 2020;8:e000244.
- Porta C, Consonni FM, Morlacchi S, et al. Tumor-derived prostaglandin E2 promotes p50 NF- $\kappa$ B-dependent differentiation of monocytic MDSCs. *Cancer Res* 2020;80:2874–88.
- Barberi T, Martin A, Suresh R, et al. Absence of host NF- $\kappa$ B p50 induces murine glioblastoma tumor regression, increases survival, and decreases T-cell induction of tumor-associated macrophage M2 polarization. *Cancer Immunol Immunother* 2018;67:1491–503.
- Wang DJ, Ratnam NM, Byrd JC, et al. NF- $\kappa$ B functions in tumor initiation by suppressing the surveillance of both innate and adaptive immune cells. *Cell Rep* 2014;9:90–103.
- Garg B, Giri B, Modi S, et al. Nfkb in pancreatic stellate cells reduces infiltration of tumors by cytotoxic T cells and killing of cancer cells, via up-regulation of CXCL12. *Gastroenterology* 2018;155:880–91. e888.

- 12 Porta C, Ippolito A, Consonni FM, *et al.* Protumor steering of cancer inflammation by p50 NF- $\kappa$ B enhances colorectal cancer progression. *Cancer Immunol Res* 2018;6:578–93.
- 13 Dong MB, Wang G, Chow RD, *et al.* Systematic immunotherapy target discovery using genome-scale in vivo CRISPR screens in CD8 T cells. *Cell* 2019;178:1189–204. e1123.
- 14 Grinberg-Bleyer Y, Oh H, Desrichard A, *et al.* NF- $\kappa$ B c-Rel is crucial for the regulatory T cell immune checkpoint in cancer. *Cell* 2017;170:1096–108. e1013.
- 15 Oh H, Grinberg-Bleyer Y, Liao W, *et al.* An NF- $\kappa$ B transcription-factor-dependent lineage-specific transcriptional program promotes regulatory T cell identity and function. *Immunity* 2017;47:450–65. e455.
- 16 Barnes SE, Wang Y, Chen L, *et al.* T cell-NF- $\kappa$ B activation is required for tumor control in vivo. *J Immunother Cancer* 2015;3:1.
- 17 Karban AS, Okazaki T, Panhuysen CIM, *et al.* Functional annotation of a novel NFKB1 promoter polymorphism that increases risk for ulcerative colitis. *Hum Mol Genet* 2004;13:35–45.
- 18 Lewander A, Butchi AKR, Gao J, *et al.* Polymorphism in the promoter region of the NFKB1 gene increases the risk of sporadic colorectal cancer in Swedish but not in Chinese populations. *Scand J Gastroenterol* 2007;42:1332–8.
- 19 O'Reilly LA, Putoczki TL, Mielke LA, *et al.* Loss of NF- $\kappa$ B1 causes gastric cancer with aberrant inflammation and expression of immune checkpoint regulators in a STAT-1-dependent manner. *Immunity* 2018;48:570–83. e578.
- 20 Hopewell EL, Zhao W, Fulp WJ, *et al.* Lung tumor NF- $\kappa$ B signaling promotes T cell-mediated immune surveillance. *J Clin Invest* 2013;123:2509–22.
- 21 Muthuswamy R, Berk E, Junecko BF, *et al.* NF- $\kappa$ B hyperactivation in tumor tissues allows tumor-selective reprogramming of the chemokine microenvironment to enhance the recruitment of cytolytic T effector cells. *Cancer Res* 2012;72:3735–43.
- 22 Lu C, Yang D, Klement JD, *et al.* Suv39H1 represses the expression of cytotoxic T-lymphocyte effector genes to promote colon tumor immune evasion. *Cancer Immunol Res* 2019;7:414–27.
- 23 Redd PS, Lu C, Klement JD, *et al.* H3K4me3 mediates the NF- $\kappa$ B p50 homodimer binding to the *pdc1* promoter to activate PD-1 transcription in T cells. *Oncimmunology* 2018;7:e1483302.
- 24 Burkitt MD, Hanedi AF, Duckworth CA, *et al.* NF- $\kappa$ B1, NF- $\kappa$ B2 and c-Rel differentially regulate susceptibility to colitis-associated adenoma development in C57BL/6 mice. *J Pathol* 2015;236:326–36.
- 25 Puar Y, Shanmugam M, Fan L, *et al.* Evidence for the involvement of the master transcription factor NF- $\kappa$ B in cancer initiation and progression. *Biomedicines* 2018;6:82.
- 26 Tergaonkar V. Nfkb drives TERT promoter reactivation in cancer. *Cell Cycle* 2016;15:156–7.
- 27 Li Y, Zhou Q-L, Sun W, *et al.* Non-canonical NF- $\kappa$ B signalling and ETS1/2 cooperatively drive C250T mutant TERT promoter activation. *Nat Cell Biol* 2015;17:1327–38.
- 28 Luo J-L, Maeda S, Hsu L-C, *et al.* Inhibition of NF- $\kappa$ B in cancer cells converts inflammation-induced tumor growth mediated by TNF $\alpha$  to TRAIL-mediated tumor regression. *Cancer Cell* 2004;6:297–305.
- 29 Thaker YR, Raab M, Strebhardt K, *et al.* Gtpase-activating protein Rasal1 associates with ZAP-70 of the TCR and negatively regulates T-cell tumor immunity. *Nat Commun* 2019;10:4804.
- 30 Gilmore TD. Introduction to NF- $\kappa$ B: players, pathways, perspectives. *Oncogene* 2006;25:6680–4.
- 31 Spranger S, Bao R, Gajewski TF. Melanoma-intrinsic  $\beta$ -catenin signalling prevents anti-tumour immunity. *Nature* 2015;523:231–5.
- 32 Juneja VR, McGuire KA, Manguso RT, *et al.* Pd-L1 on tumor cells is sufficient for immune evasion in immunogenic tumors and inhibits CD8 T cell cytotoxicity. *J Exp Med* 2017;214:895–904.
- 33 Zappasodi R, Budhu S, Hellmann MD, *et al.* Non-conventional inhibitory CD4+Foxp3–PD-1hi T cells as a biomarker of immune checkpoint blockade activity. *Cancer Cell* 2018;33:1017–32. e1017.
- 34 Larkin J, Chiarion-Sileni V, Gonzalez R, *et al.* Five-year survival with combined nivolumab and ipilimumab in advanced melanoma. *N Engl J Med* 2019;381:1535–46.
- 35 Rizvi NA, Hellmann MD, Snyder A, *et al.* Cancer immunology. mutational landscape determines sensitivity to PD-1 blockade in non-small cell lung cancer. *Science* 2015;348:124–8.
- 36 Sun Z, Arendt CW, Ellmeier W, *et al.* Pkc-theta is required for TCR-induced NF- $\kappa$ B activation in mature but not immature T lymphocytes. *Nature* 2000;404:402–7.
- 37 Farren MR, Sayegh L, Ware MB, *et al.* Immunologic alterations in the pancreatic cancer microenvironment of patients treated with neoadjuvant chemotherapy and radiotherapy. *JCI Insight* 2020;5:e130362.
- 38 Mace TA, Shakya R, Pitarresi JR, *et al.* IL-6 and PD-L1 antibody blockade combination therapy reduces tumour progression in murine models of pancreatic cancer. *Gut* 2018;67:320–32.
- 39 Kleffel S, Posch C, Barthel SR, *et al.* Melanoma cell-intrinsic PD-1 receptor functions promote tumor growth. *Cell* 2015;162:1242–56.
- 40 Lee N, Zakka LR, Mihm MC, *et al.* Tumour-infiltrating lymphocytes in melanoma prognosis and cancer immunotherapy. *Pathology* 2016;48:177–87.
- 41 Miller BC, Sen DR, Al Abosy R, *et al.* Subsets of exhausted CD8<sup>+</sup> T cells differentially mediate tumor control and respond to checkpoint blockade. *Nat Immunol* 2019;20:326–36.
- 42 Barham W, Gicobi JK, Yan Y, *et al.* Paradox-driven adventures in the development of cancer immunology and immunotherapy. *Genes Dis* 2019;6:224–31.
- 43 Liu X, Gibbons RM, Harrington SM, *et al.* Endogenous tumor-reactive CD8<sup>+</sup> T cells are differentiated effector cells expressing high levels of CD11a and PD-1 but are unable to control tumor growth. *Oncimmunology* 2013;2:e23972.
- 44 Wolchok JD, Kluger H, Callahan MK, *et al.* Nivolumab plus ipilimumab in advanced melanoma. *N Engl J Med* 2013;369:122–33.
- 45 Gerondakis S, Fulford TS, Messina NL, *et al.* NF- $\kappa$ B control of T cell development. *Nat Immunol* 2014;15:15–25.
- 46 Vivier E, Artis D, Colonna M, *et al.* Innate lymphoid cells: 10 years on. *Cell* 2018;174:1054–66.
- 47 Kirchberger S, Royston DJ, Boulard O, *et al.* Innate lymphoid cells sustain colon cancer through production of interleukin-22 in a mouse model. *J Exp Med* 2013;210:917–31.
- 48 Vallentin B, Barlogis V, Piperoglou C, *et al.* Innate lymphoid cells in cancer. *Cancer Immunol Res* 2015;3:1109–14.
- 49 Xie S, Li J, Wang JH, *et al.* Il-17 activates the canonical NF- $\kappa$ B signaling pathway in autoimmune B cells of BXD2 mice to upregulate the expression of regulators of G-protein signaling 16. *J Immunol* 2010;184:2289–96.
- 50 Schwartz C, Khan AR, Floudas A, *et al.* Ilc2S regulate adaptive Th2 cell functions via PD-L1 checkpoint control. *J Exp Med* 2017;214:2507–21.

## Supplemental Data

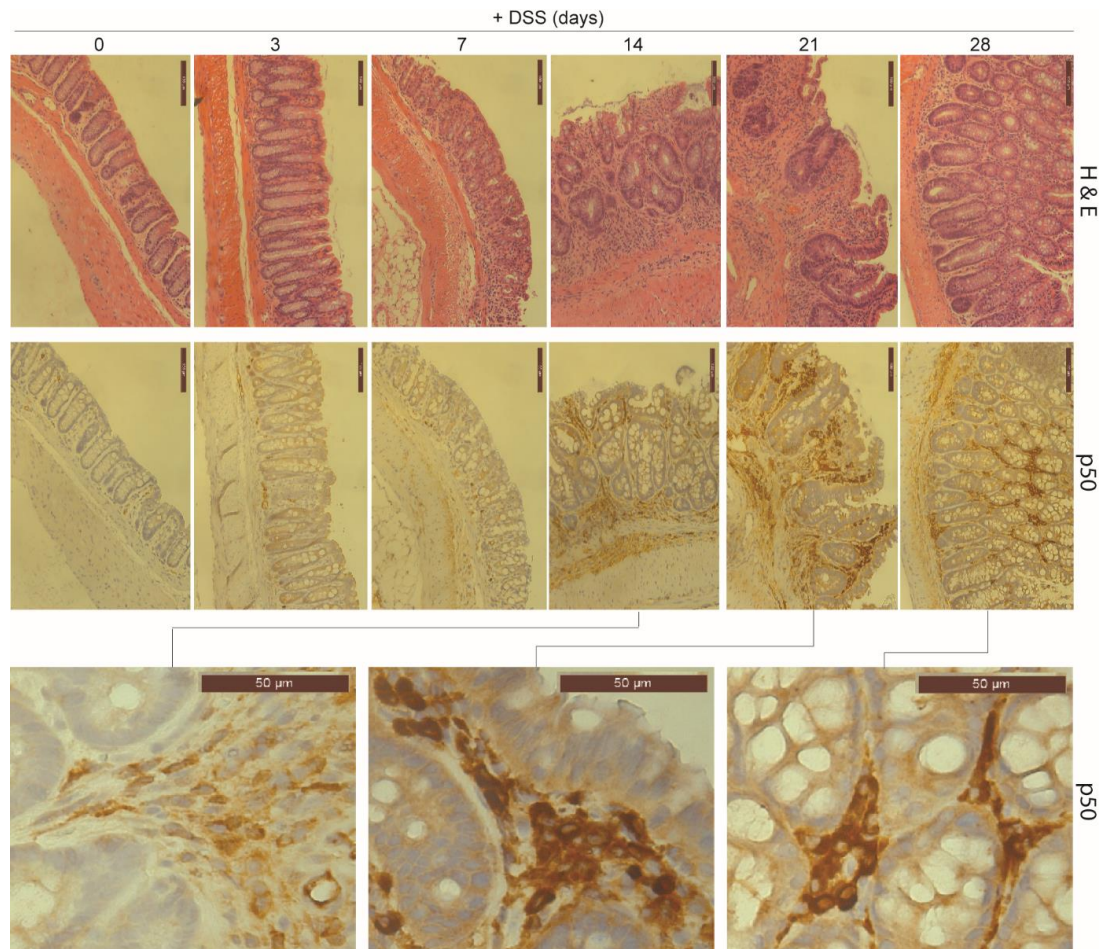


**Figure S1. Colonic inflammation induces p50 NF- $\kappa$ B activation primarily in colon lamina propria immune cells.** WT mice were treated with the DSS-water cycle as in Fig2. A and C. Colon tissues were collected at the indicated time points, and prepared as SWISS rolls. The SWISS rolls were fixed, paraffin-embedded, and sectioned. The sections were stained with H & E (upper panel), and p50-specific antibody (middle panel), respectively. The bottom panel shows magnified images of p50-stained colon tissues.

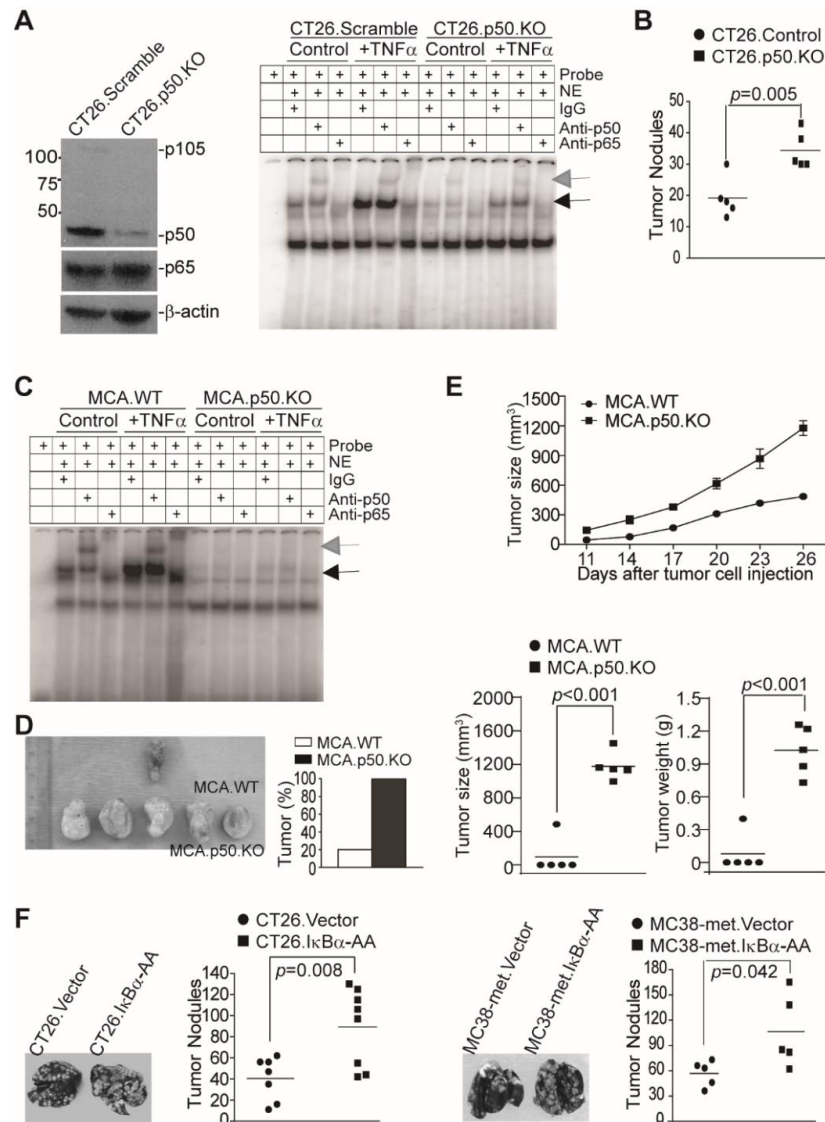


**Figure S2. p50 NF- $\kappa$ B acts as a tumor suppressor in tumor cells in vivo.** **A.** CT26 cells were transduced with lentiviral particles containing CRISPR vectors with scramble and *Nfkb1*-specific gRNA-coding sequences, respectively, and selected for stable cell lines. The resultant CT26.Scramble and CT26.p50.KO cells were first analyzed by Western for p50 and p65 protein levels (left panel), and then by EMSA after treatment with TNF $\alpha$  for 1h (right panel). Anti-p50 and anti-p65 antibodies were used to determine p50 and p65 NF- $\kappa$ B activation. **B.** CT26.Scramble and CT26.p50.KO cells were injected i.v. into Balb/c mice. Tumor-bearing lungs were collected 14 days later, inflated with India ink, fixed, and enumerated for tumor nodule numbers. **C.** Tumors were dissected from the MCA-induced tumors in WT and p50 KO mice as shown in Fig. 2B. Stable tumor cell lines were established from the tumors. The p50 WT (MCA.WT) and p50-deficient (MCA.p50.KO) cells were analyzed by EMSA for NF- $\kappa$ B activation as in A. **D.** MCA.WT and MCA.p50.KO cells were injected s.c. to C57BL/6 mice and analyzed for tumor

growth. Shown are tumor image 26 days after tumor cell injection (left panel), tumor incidence (right panel). **E.** Tumors as shown in D were monitored for growth kinetics (top panel). The tumor size and weight were measured at the end of the experiments (bottom panels). **F.** CT26.Vector and CT26.I $\kappa$ B $\alpha$ -AA cells (left two panels) were injected i.v. into Balb/c mice. MC38-met.Vector and MC38-met.I $\kappa$ B $\alpha$ -AA cells were injected i.v. to C57BL/6 mice (right two panels). Lung metastasis was analyzed 14 days after tumor cell injection. Shown are representative images of tumor-bearing lungs of CT26.Vector and CT26.I $\kappa$ B $\alpha$ -AA, as well as MC38-met.Vector and MC38-met.I $\kappa$ B $\alpha$ -AA tumors. The tumor nodule number was quantified and presented on the right.

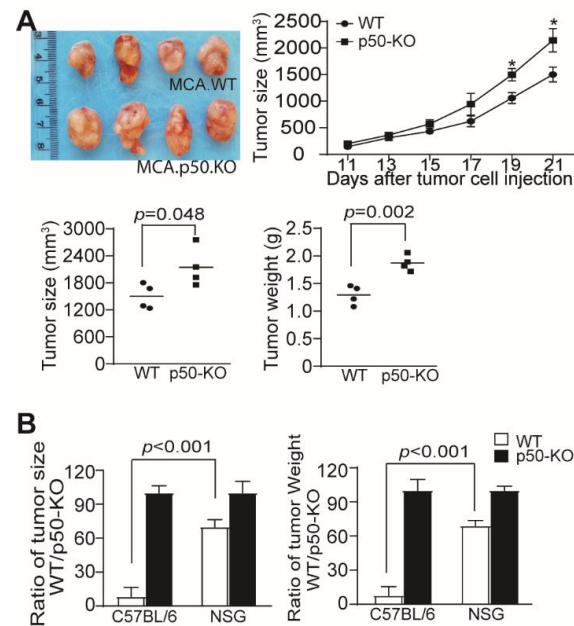


**Figure S3. p50 NF- $\kappa$ B function in immune cells significantly outweighs its function in tumor cells.** **A.** MCA.WT and MCA.p50.KO tumor cells were injected s.c. to NSG mice. Shown are tumor images (top left panel) and growth kinetics (top right panel). Mice were sacrificed 21 days after tumor cell injection and measured for tumor size and weight (bottom panels). **B.** The tumor size (left panel) and tumor weight (right panel) of MCA.p50.KO tumors in C57BL/6 and NSG mice as shown in Fig. S2D and S3A, respectively, were arbitrarily set to 100%. The tumor size and weight of the respective MCA.WT tumors were then calculated as % of the respective MCA.p50 KO tumors.

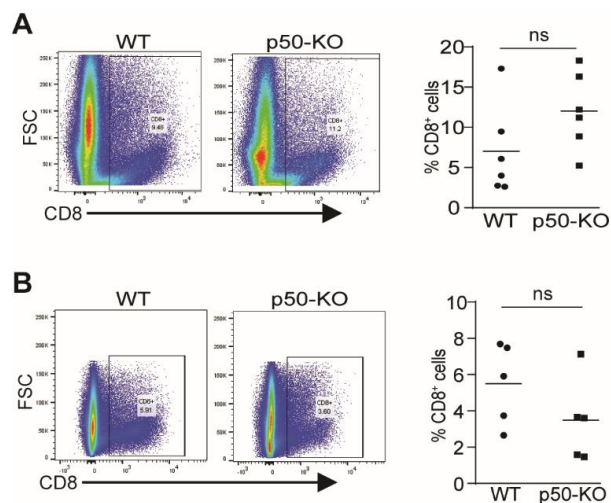


**Figure S4. Tumor-infiltrating CTL profiles in WT and p50 KO mice.** **A.** Tumor tissues were collected from subcutaneous MC38 tumor-bearing mice WT (n=6) and p50 KO (n=6) mice, digested with collagenase to make single cells. Cell mixtures were stained for live cells with DAPI and mAb for CD8, and analyzed by flow cytometry. The gated live cells were then analyzed for CD8<sup>+</sup> T cells. Shown are representative dot plots (left panel). The CD8<sup>+</sup> T cells among the total live cells were quantified (right panel). **B.** Orthotopic MC38 colon tumors (n=5) were analyzed as in A above for CD8<sup>+</sup> tumor-infiltrating T cells.

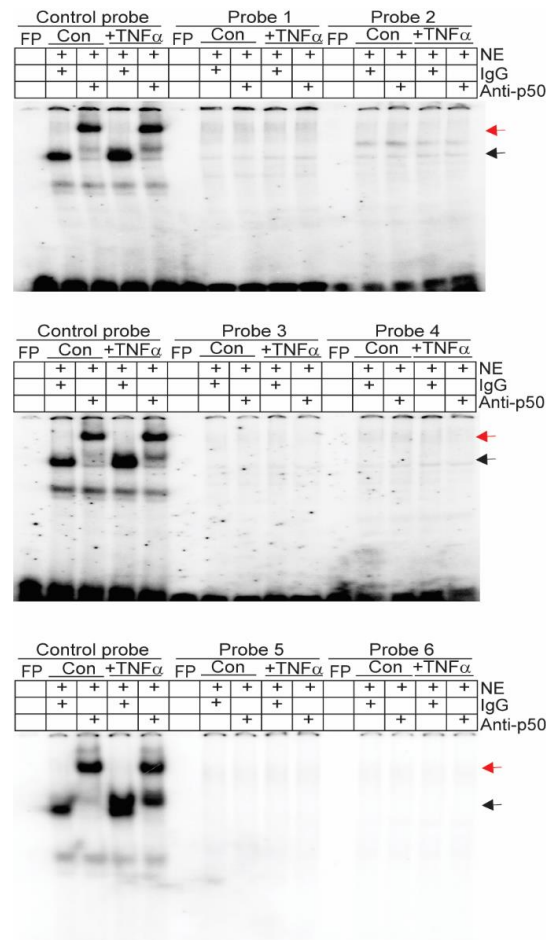


**Figure S5. Identification of p50-binding site in the *Gzmb* promoter in T cells.** Nuclear extracts were prepared from EL4 T cells and analyzed by EMSA using the 6 putative *Gzmb* promoter DNA probes (probes 1-6) as shown in Figure 4A. The NF- $\kappa$ B consensus sequence probe (control probe) was used as positive control in each gel. The black arrows indicates the NF- $\kappa$ B-DNA complex and the red arrows indicates p50 mAb-induced supershift.

**Table S1. Patient pathological report**

Case Number	Gender	Age	Type	Description	Tumor	Treatment
00SL03016498	Male	73	colon, transverse and liver	moderately differentiated adenocarcinoma, with liver metastasis	primary	Chemotherapy
00SL03023527	Male	55	rectosigmoid junction	moderately to poorly differentiated adenocarcinoma, with liver metastasis	primary	Chemotherapy and radiation
00SL03033974	Male	57	colon, ascending and liver	moderately differentiated adenocarcinoma, liver metastasis.	primary	Chemotherapy and radiation
00SF05027627	Male	75	colon, ascending and liver	adenocarcinoma of the colon, grade 1. Liver metastasis	primary	Chemotherapy adjuvant
00SL06001063	Male	64	colon, cecum, liver	adenocarcinoma, liver metastasis	primary	Radiation therapy and chemotherapy
00SL08019545	Female	70	colon, hepatic flexure	moderately differentiated adenocarcinoma	primary	Adjuvant chemotherapy and radiation
00SL09014173	Male	87	colon	moderately differentiated adenocarcinoma of sigmoid colon,	primary	Neoadjuvant chemoradiotherapy
00SL09026220	Male	79	colon, liver	adenocarcinoma, low grade moderately differentiated. Liver metastasis	primary	Chemoradiation therapy
00SL11013083	Female	28	colon, peritoneum	adenocarcinoma with signet ring cells with diffuse peritoneal metastases	primary	Adjuvant chemotherapy and radiation
00SL12040817	Male	40	rectum, sigmoid	invasive carcinoma of the sigmoid colon with liver metastasis	primary	Chemotherapy adjuvant

**Table S2. PCR Primers**

Primers	Sequence
mIL6-F	TCTGGGAAATCGTGGAAATGAG
mIL6-B	TCTCTGAAGGACTCTGGCTTTGTC
mVwa2-F	AACGCCTGAGCAGAGGGTTC
mVwa2-B	CTGGGAAAACGGACTCCTACG
mMyo3a-F	AAGAGGGGAGAAAGAATGAGCG
mMyo3a-B	TCACGGTGGATGGTTTTGTTG
mCXCL10-F	TCTCTCCATCACTCCCCTTTACC
mCXCL10-B	CTTGCTTCGGCAGTTACTTTTGTC
mCcl11-F	GCTTCTATTCTGCTGCTCACG
mCcl11-B	TCTTTGCCCAACCTGGTCTTG
mCcl4-F	TGCCTTCTGTGCTCCAGGGTTC
mCcl4-B	TGCCTCTTTTGGTCAGGAATACC
mGZMB-F	GCCCACAACATCAAAGAACAGG
mGZMB-B	CCAACCAGCCACATAGCACAC
mAlox12e-F	TACAGTCACATCTGCTGAGGGGAC
mAlox12e-B	TATTCCTGCGCCAGGGTGTG
mGnao1-F	GGGCTGGAGAATCAGGAAAAAG
mGnao1-B	GACTGGATGGTGTGCTGTAGACC
mCcl12-F	TCCTCAGGTATTGGCTGGACC
mCcl12-B	CACTGGCTGCTTGTGATTCTCC
mAlox15-F	AGGGAGGAGGAACTGGAAGAAAG
mAlox15-B	AGGGAGGTCAGAGATACTGGTCGC
mIRF4-F	GACGACAATGGACAGAGGAAGAAC
mIRF4-B	GCACAGAGTCACCTGGAATCTCG
mIL17A-F	CCCTCAGACTACCTCAACCGTTC
mIL17A-B	TCTCAGGCTCCCTCTTCAGGAC
mCd3d-F	AAAGGCGTTCTGGACCCACG
mCd3d-B	CACACAGTTCTGGCACATTCGG
mH2-Oa-F	CAGAGTGGGCTGATGAGCATTTC
mH2-Oa-B	GAGTCTTGGGGAGAACGGTCAC
mAlox12-F	GCTTACCTCAGACAATAGCAGCG
mAlox12-B	ACACTGGTGAACCTTCTCGGC
mCcl2-F	CCCAATGAGTAGGCTGGAGAGC
mCcl2-B	TGGTTGTGGAAAAGGTAGTGGATG
m $\beta$ Actin-F	ATTGTTACCAACTGGGACGACATG
m $\beta$ Actin-B	CTTCATGAGGTAGTCTGTCAGGTC
mGzmB-NF $\kappa$ B ChIP-F	CCTCGGCAGAACTGTAAAGGC
mGzmB-NF $\kappa$ B ChIP-B	GCTGGACATCCTAATCTTCACTGAC

**Table S3. Antibodies**

Antibody	Source	Clone	Cat Number	Application
FITC anti-mouse CD8	Biolegend	53-6.7	100706	Flow Cytometry
PerCP anti-mouse CD8	Biolegend	53-6.8	100732	Flow Cytometry
Pacific Blue anti-human/mouse GzmB	Biolegend	GB11	515408	Flow Cytometry
PE-Cy7 anti-mouse CD45.2	Biolegend	104	109830	Flow Cytometry
APC-Cy7 anti-mouse PD1	Biolegend	29F.1A12	135224	Flow Cytometry
Zombie UV	Biolegend		423108	Flow Cytometry
MojoSort Mouse CD45 Nanobeads	Biolegend		480108	Cell isolation
p50	Santa Cruz	E-10	sc-8414	Immunohistochemistry
p105/p50	Biolegend	W16200A	603901	WB
p65	Cell Signaling Technology	D14E12	8242P	WB
Normal Rabbit IgG	Cell Signaling Technology		2729P	ChIP
Normal Rabbit IgG	R&D Systems		AB-105-C	EMSA
p50	Santa Cruz	E-10	sc-114X	EMSA, ChIP
p65	Santa Cruz	C20	sc-372X	EMSA
p52	Santa Cruz	C5	sc-7386X	EMSA
c-Rel	Santa Cruz	N	sc-70X	EMSA
Rel B	Santa Cruz	C19	sc-226X	EMSA
rmTNF $\alpha$	R&D Systems		410-MT	In vitro treatment

**Table S4: Two-Factor ANOVA Results on Tumor Volume and Weight between Strain and Treatment**

Outcome	Mouse Strain	Treatment	Mean (SD)	F	p-value
Tumor Volume	WT		2121.12 (1574.90)	1.83	0.1952
	p50KO		1609.75 (469.13)		
		Anti-PD1	1382.41 (516.73)	6.52	0.0212
		IgG	2348.46 (1435.33)		
	WT	Anti-PD1	998.07 (374.43)	11.45	0.0038
		IgG	3244.16 (1512.42)		
	p50KO	Anti-PD1	1766.76 (302.15)		
		IgG	1452.75 (585.04)		
Tumor Weight	WT		2.14 (1.34)	1.26	0.2789
	p50KO		1.82 (0.57)		
		Anti-PD1	1.48 (0.61)	12.26	0.0030
		IgG	2.49 (1.12)		
	WT	Anti-PD1	1.03 (0.42)	18.21	0.0006
		IgG	3.26 (0.87)		
	p50KO	Anti-PD1	1.93 (0.37)		
		IgG	1.71 (0.76)		